Lab on a Chip

Accepted Manuscript

ROYAL SOCIETY OF CHEMISTRY

www.rsc.org/loc

Journal Name

RSCPublishing

ARTICLE

Ultrafast immunoassays by coupling dielectrophoretic biomarker enrichment on nanoslit molecular dam with electrochemical detection on graphene

Cite this: DOI: 10.1039/x0xx00000x

Received 00th September 2013,
Accepted 00th September 2013

DOI: 10.1039/x0xx00000x

www.rsc.org/

Bankim J. Sanghavi[a], Walter Varhue[a], Ali Rohani[a], Kuo-Tang Liao[b], Lindsay Bazydlo[c], Chia-Fu Chou[b]*, Nathan S. Swami[a]*

Heterogeneous immunoassays usually require long incubation times to promote specific target binding and several wash steps to eliminate non-specific binding. Hence, signal saturation is rarely achieved at detection limit levels of analyte, leading to significant errors in analyte quantification due to extreme sensitivity of the signals to incubation time and methodology. The poor binding kinetics of immunoassays at detection limit levels can be alleviated through creating an enriched analyte plug in the vicinity of immobilized capture probes to enable signal saturation at higher levels and at earlier times, due to higher analyte association and its faster replenishment at the binding surface. Herein, we achieve this by coupling frequency-selective dielectrophoretic molecular dam enrichment of the target biomarker in physiological media to capture probes immobilized on graphene-modified surfaces in a nanoslit to enable ultrafast immunoassays with near-instantaneous (< 2 minutes) signal saturation at dilute biomarker levels (picomolar) within ultra-low sample volumes (picoliters). This methodology is applied to the detection of Prostate Specific Antigen (PSA) diluted in serum samples, followed by validation against a standard two-step immunoassay using three de-identified patient samples. Based on the ability of dielectrophoretic molecular dam analyte enrichment methods to enable the detection of PSA at 1-5 pg/mL levels within a minute, and the relative insensitivity of the signals to incubation time after the first two minutes, we envision its application for improving the sensitivity of immunoassays and their accuracy at detection limit levels.

1 Introduction

Heterogeneous immunoassays utilizing antibody sandwich formats on nanoparticles are widely applied for detecting various protein and small molecule biomarkers at high levels of sensitivity and specificity [1-3]. However, these assays usually require long incubation times to promote specific binding and several wash steps to eliminate non-specific binding. Additionally, conventional immunoassay methodologies are not well suited for working with the sub-nanoliter level sample volumes often encountered within point-of-care diagnostic and therapeutic applications, such as for the serial monitoring of cells from liquid biopsies [4]. Due to the large association constants of these high-affinity immunoassays, the analyte binding kinetics are limited by mass transport rather than chemical reaction rate [5], which greatly increases target settling time [6]. This bottleneck is especially accentuated at biomarker levels below their antibody dissociation constant (sub-nanomolar levels for Prostate Specific Antigen or PSA [7, 8]) and within ultra-low sample volumes. Hence, immunoassay signals do not saturate within the measurement time, leading to greater variations in analyte quantification due to the sensitivity of signals to incubation time and method. The slow binding kinetics within dilute analyte samples also limit the dynamic range of the sensor and that of the flow rates applied to enhance sample throughput and/or alleviate mass transport limitations.

The implementation of immunoassays within microfluidic platforms by using a critical level of analyte flow to replenish its depletion at the binding surface has been widely proposed as a means to address the mass transport bottlenecks [9, 10]. Based on models of binding kinetics under flow within microfluidic systems, the early saturation of signals has been predicted for enabling greater accuracy of analyte quantification due to lower sensitivity of signals to assay time [11]. However, the benefits of these microfluidic flow methods need to be weighed against the available sample volume and the limitations on analyte flow rate imposed by the residence times required to enable analyte binding [5]. Furthermore, methods to enhance analyte exploitation by increasing the overall volumetric flow rate are less effective within nanosensor geometries that display high sensitivity, since the level of analyte depletion is low, due to the fewer capture probes [12].

An alternate microfluidic approach is based on actively steering analytes towards the sensing region, since analyte capture from a concentrated plug of low volume is more effective than that from a dilute plug of large volume, even upon continued re-circulation [13]. A commonly investigated methodology for achieving highly concentrated analyte plugs from dilute samples is through electrokinetic enrichment due to ion depletion at the micro/nanochannel interface [14]. In this manner, by pre-immobilizing antibodies within the region with the enriched reporter molecules [15], the detection of Prostate Specific Antigen biomarkers at ~1.85 pg/mL has been demonstrated within just 30 minutes [16]. Analyte binding kinetics can also be enhanced by immobilizing capture probes inside nanoslit channels [17, 18], since high radial diffusion within the confined device geometry significantly lowers extent of the diffusion layer. However, no prior work has combined the two approaches by applying electrokinetic enrichment of the biomarkers inside nanoslit device geometries with locally immobilized capture probes, to explore the enhancement in analyte binding kinetics arising from the synergies. This is challenging since it requires the patterning of intact capture probes in the nanoslit for measuring immunoassay binding kinetics at short time intervals, with detection limit analyte levels and in the absence of intervening wash steps.

Herein, we demonstrate the feasibility for ultrafast immunoassays through directly coupling dielectrophoretic molecular dam enrichment of PSA biomarkers to capture probes immobilized in a nanoslit channel. Frequency-selective negative dielectrophoresis (nDEP) alongside DC electrokinetic transport is chosen for enabling the enrichment of polarized biomarkers to create a highly concentrated plug of the biomarker within the localized region containing immobilized antibodies in the nanoslit. While prior work on immunoassays has utilized electrode-based nDEP to indirectly enrich biomarkers by localizing microbeads immobilized with the target antigen [19, 20], we instead utilize electrode-less nDEP, since it can directly enrich biomarkers within physiological media to create highly concentrated analyte plugs from dilute samples, by using sharp insulator constrictions inside a nanoslit channel under a molecular dam scheme [21, 22]. Specifically, under an AC field of ~200 V_{pp}/cm at 6 MHz frequencies, PSA molecules are enriched by nDEP away from the field non-uniformity created by the tips of sharp constrictions. While our prior work utilized a similar methodology of nDEP molecular dam enrichment of neuropeptides at 3 MHz for enabling more sensitive detection of their electro-oxidation current [23], this enrichment was not coupled to capture probes immobilized in the molecular dam region, which is a significant challenge. Here, on the other hand, anti-PSA probes are immobilized in the PSA enrichment region on gold nanoparticles (AuNPs) to enable selectivity and on an underlying graphene modified glassy carbon surface with high adsorption and electron transfer kinetics for electroactive species, to enhance sensitivity [24]. Additionally, since electron transfer rates steeply drop-off for electroactive molecules localized beyond a few nanometers from the electrode surface, a wash step to remove excess secondary antibody or reporter molecules is not needed. In this manner, standard voltammetric methods can be applied to follow the binding kinetics of PSA to anti-PSA under the molecular dam scheme within the nanoslit. While our prior work has observed the dielectrophoretic enhancement of DNA hybridization kinetics [25-27], the realization of ultrafast immunoassays reported herein required the integration of nanofluidic device geometries [28], biofunctional nanoslit bonding methods [29], spatio-temporal image analysis [30] and high-frequency amplifiers [31] for optimizing nDEP enrichment of nanoscale biomarkers in physiological media. This methodology to alleviate target transport limitations at detection limit levels can be applied in complement with other reported strategies for enhancing PSA detection sensitivity, such as through improved capture probe immobilization [32], or through post target-binding signal amplification strategies [33], for eventually enhancing detection accuracy by enabling signal saturation at earlier times. Based on the ultrafast saturation of signals (~2 minutes) from dilute biomarker samples (picomolar levels) within ultra-low sample volumes (picoliters), we envision significant opportunities for enhancing the sensitivity and accuracy of immunoassays in general.

2 Materials and Methods

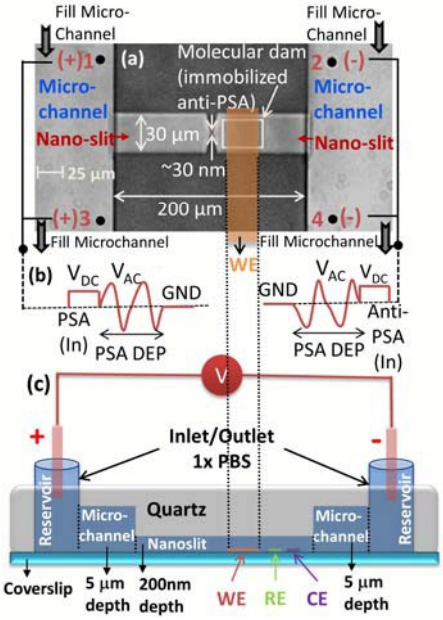

Fig. 1: Nanoslit device: (a) Top-view of microchannels leading to nanoslit with lateral constrictions aligned to the molecular dam region with immobilized anti-PSA, (b) electrical signal sequence at inlet/outlet ports 1 & 3 (left) versus 2 & 4 (right) after filling microchannels with PSA and NPP (left), and ALP-tagged anti-PSA (right); and (c) cross-sectional view of nanoslit bonded to glass cover slip patterned with working (WE), reference (RE) and counter electrodes (CE). The positive (left) and negative (right) indicates net DC offset during nDEP.

Chemicals and Instrumentation

All chemicals were of A. R. grade and used without any further purification. Prostate Specific Antigen (PSA) was procured from Sigma-Aldrich and anti-PSA was obtained from Abcam. Graphite powder and Chloro-auric acid ($HAuCl_4$) were

purchased from Sigma Aldrich. All solutions were prepared using double distilled water of specific conductivity: 1-3 μS/cm). Phosphate buffer saline (PBS; 0.1 M, pH 6.5) of ~1.7 S/m conductivity was used as the supporting electrolyte, with regular conductivity and pH measurements (Mettler Toledo FE20). Electrochemical measurements were performed on Solartron Analytical's Electrochemical Station; model Modulab 2101A, equipped with a femto-Amp booster pre-amplifier.

Nanoslit device

The nanoslit device (Fig. 1) was constructed on fused silica (quartz) using photolithography and electron beam lithography for resist patterning, followed by reactive ion etching for nanofabrication of channels, as described within previous work [21, 22]. Briefly, as per the top-view in Figure 1a and the cross-section view in Figure 1c, four inlet/outlet reservoirs (labeled 1-4) lead to two microchannels (~5 μm depth) and a set of nanoslit channels (~200 nm depth), each with sharp lateral constrictions (30 μm to ~30 nm) to create field non-uniformities for nDEP trapping. Preliminary optimization of the field conditions to initiate nDEP trapping of Dylight 594 labeled PSA (AbD Serotech) using a function generator and amplifier [31] was accomplished through bonding the nanoslit to a polysilsesquioxane (PSQ) coated cover-slip [34, 35], for observation under inverted microscopy (Zeiss, Z1) using an Electron multiplier CCD (Hamamatsu).

Micropatterning and surface modification of detection electrodes

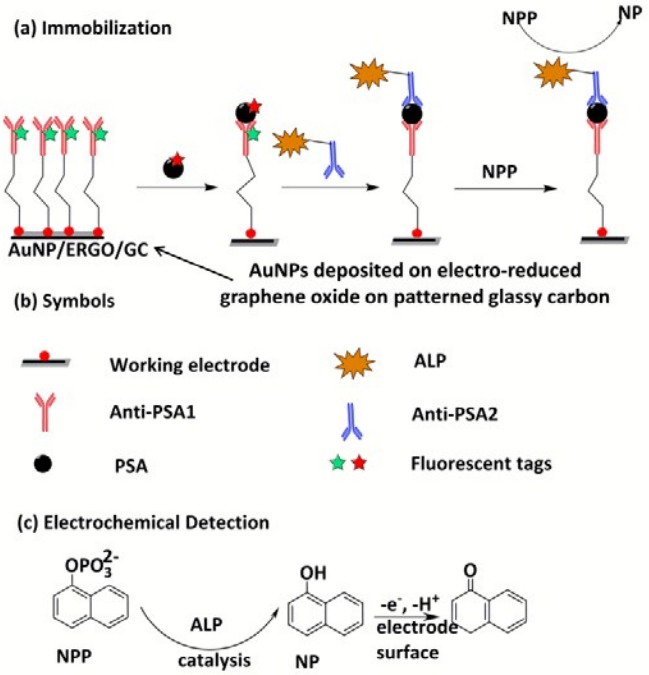

Fig. 2: Detection scheme for PSA: (a) Immobilization of anti-PSA capture probes on AuNP modified graphene/glassy carbon surfaces for a PSA sandwich assay using ALP-tagged secondary antibodies; (b) Symbols; (c) Electrochemical detection method. Note: Fluorescent tags applied only for optimizing the device and E-field for nDEP enrichment.

Following optimization of the field conditions for nDEP enrichment by imaging of fluorescently-labeled PSA, all subsequent detection was performed by electrochemical methods. As described within prior work [23], electrochemical detection electrodes were microfabricated on PSQ-coated cover-slip glass (Figure 1 c), by patterning a standard resist and converting it to glassy carbon (GC) by pyrolysis methods [36]. This was followed by electro-reduction of graphene oxide (ERGO) [37] and electrodeposition of AuNPs at -0.8 V for 60 s in 1 mM $HAuCl_4$ [38]. Alternate patterned electrodes on the cover-slip function as the reference (Ag/AgCl prepared by electrodeposition with Ag and $FeCl_3$ treatment for chloridizing the surface [39]) and counter electrodes (glassy carbon). As per the overall scheme in Figure 2a, PSA antibody was thiolated [40] for enabling immobilization on AuNP modified ERGO deposited on the glassy carbon surface. The electrodes for electrochemistry were micropatterned inside a window of the PSQ-coated cover-slip for subsequent alignment to the constriction region of the nanoslit on the fused silica substrate, for bonding at room temperature, to preserve biofunctionality of the immobilized anti-PSA capture probes [29, 35]. Prior to bonding, the length-edge of the working electrode was orthogonally aligned to be within ~5 μm from the constriction tip, to align the nDEP enrichment region of the biomarkers to the electrochemical detection electrodes. This device geometry ensures that the counter and reference electrodes are in the same nanochannel as the working electrode, thereby enabling sensitive current measurement and allowing all potential drops to occur at the surface of the working electrode, rather than in solution. Optimization of nDEP was performed using Dylight 488 labeled anti-PSA (Jackson ImmunoResearch Laboratories) and Dylight 594 labeled PSA (AbD Serotech); with no fluorescently tags in subsequent electrochemical detection.

Modification of secondary PSA antibody for sandwich assay

The sandwich assay for electrochemical detection was performed using Alkaline phosphatase (ALP) tagged to the secondary PSA antibody by glutaraldehyde coupling [41], for enabling the selective catalysis of α-naphthyl phosphate (NPP) to the electroactive α-naphthol (NP) product [40], as per the detection scheme in Figure 2c. For ALP tagging of anti-PSA, an appropriate amount of ALP solution was transferred to an Eppendorf tube and mixed with anti-PSA in deionized water. Next, 1% glutaraldehyde in 0.1 M phosphate buffer (pH 7.4) was added to the solution. The resulting mixture was incubated with shaking (120 rpm) at room temperature for 10 min, and then incubated for 4 hours in the dark. Finally, 1 M monoethanolamine solution was added to the mixture, which was subsequently incubated with shaking (100 rpm) for 2 h at room temperature. The mixture was dialyzed against PBS solution at 4 °C overnight. The dialysis product, PSA antibody-ALP conjugate, was then transferred to an Eppendorf tube and mixed with an equal volume of glycerin and 1% BSA, for storage at 0 °C, prior to the experiments.

Integrated device operation

Three types of experiments were performed to compare the binding kinetics of PSA with immobilized anti-PSA capture

probes on the AuNPs on the ERGO modified GC electrode surfaces using electrochemical detection with: (i) ~1 µL scale droplets on the microfabricated cover-slip; (ii) nanoslit device (~0.1 nL) integrated to the microfabricated cover-slip, with no nDEP enrichment; and (iii) nDEP enriched PSA within the nanoslit device integrated to the microfabricated cover-slip. For case (i), droplets of ~1 µL were incubated on SU8 patterned cover-slip with the microfabricated electrodes. For case (ii), a pulse-free flow system (neMESYS Syringe pump from Cetoni, Inc.) was used to fill microchannels, followed by application of 50 V_{DC} at glassy carbon modified Pt electrodes (Alfa Aesar) within each inlet/outlet reservoir for electrokinetic sample transport into the nanoslit. For case (iii), electrodes at the reservoirs were programmed to a sequence of electrical signals [42], as indicated in Figure 1b, with terminals (1) and (3) (left) versus (2) and (4) (right). The sequence involves a DC field of 50 V/cm for 10 s to enable electrokinetic filling of PSA (concentration varied from 1 pg/mL – 5 ng/mL) and NPP (100 mM) from the reservoirs, followed by the time period for which nDEP was conducted using ~200 V_{pp}/cm at 6 MHz with a DC offset of 1.5 V/cm, and finally, a DC field (50 V/cm for 5 s) to enable electrokinetic filling ALP-tagged secondary anti-PSA and BSA from the reservoirs into the nanoslit. Square-wave voltammetric (SWV) scans of α-NP were performed in the pH 6.5 PBS media by scanning from 0.1 to 0.4 V_{DC}, using a 100 Hz frequency; 4 mV step potential; and 25 mV AC amplitude. The time on the kinetic plots is the time for PSA DEP (under AC field) plus the short time for transport of secondary antibody to the nanoslit (~5 s of V_{DC}). Solely for the case of analysis within the 1 µL droplet, a short accumulation time (10 s) at a deposition potential of -0.1 V was used to enhance adsorption. Standard deviations (95% confidence levels) were based on three different electrochemical measurements at each time point for each of the PSA concentration levels reported herein.

PSA analysis in serum samples

Serum samples were provided as de-identified and discarded samples from the University of Virginia Health System Medical Laboratory, with PSA levels measured using the total PSA 2-step immunoassay by Abbott, analyzed on an Abbott Architect. Since serum samples ranged in the 1.1-1.2 S/m range, its dilution within a higher salt media was necessary to cause a net media conductivity of 1.5-1.6 S/m, which is required for voltammetry measurements. The dilution plot to determine signal versus PSA level was measured by spiking PSA into female serum samples, so that the net PSA levels ranged from 1 pg/mL to 5 ng/mL; within media of ~1.5 S/m conductivity. To improve the signal to noise for voltammetry within diluted serum samples, the acquisition time was increased for greater signal averaging. To prevent clogging of the nanoslit, particles of ≥ 0.2 µm size were filtered from the diluted serum using Amicon Ultrafilters (EMD Millipore). During device operation, BSA was added to reduce non-specific binding [43, 44], while a dilute suspension of pre-extracted lipid vesicles [45] was added prior to PSA introduction, to reduce stochastic PSA binding at the defect regions of the nanoslit. Each de-identified serum sample was diluted ten-fold within PBS media to raise media conductivity to ~1.5 S/m and PSA levels of the original samples were reported by comparing signals to those from standard PSA samples with equivalent dilution, for enabling validation against analysis on the Abbott Architect system.

3 Results and Discussion

Optimizing nDEP enrichment of PSA

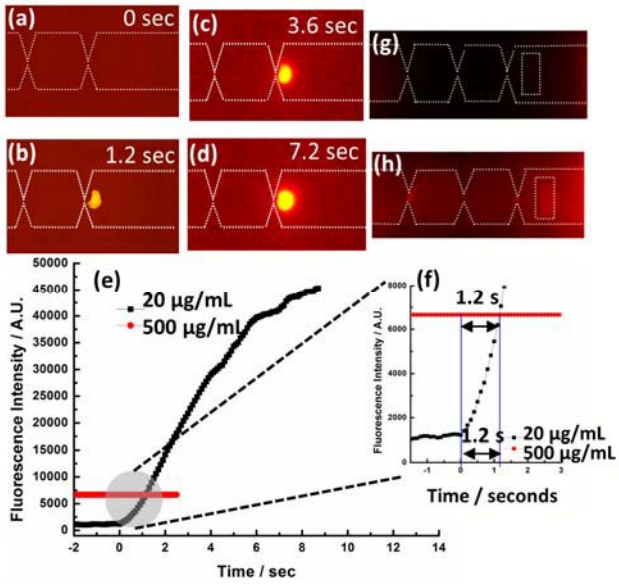

Fig. 3: Enrichment of fluorescently labelled PSA biomarkers by negative dielectrophoresis (nDEP) away from constrictions in the nanoslit: (a)-(d) images at indicated nDEP time intervals; (e) Average of maximum intensities from 20 pixels in nanoslit; (f) shows ~25x enrichment in ~1 s (black: 20 µg/mL PSA under nDEP; red: 500 µg/mL PSA with no enrichment). Binding of nDEP enriched PSA to immobilized anti-PSA capture probes in nanoslit: (g) before and (h) after PSA enrichment (2 minutes).

The optimization of field conditions for nDEP enrichment of PSA, in conjunction to its effective binding to immobilized anti-PSA within the nanoslit device are confirmed using fluorescently labeled biomarkers. For this purpose, Dylight 488 labeled anti-PSA is immobilized over a patch on cover-slip glass that is aligned to the region with maximum biomarker enrichment under nDEP (~5 µm from constriction tips inside nanoslit as per Figure 1a). The fluorescence images in Figure SI-1 of intact immobilized anti-PSA capture probes and their binding with Dylight 594 labeled PSA (20 µg/mL) confirm that biofunctionality is preserved within the nanoslit after device bonding and assembly. After optimization of the applied field at ~200 V_{pp}/cm at 6 MHz, we show the highly effective enrichment of Dylight 594 labeled PSA (starting level of 20 µg/mL) in Figure 3a-3d. In fact, the fluorescence signal reaches a level equivalent to that from 500 µg/mL PSA (determined based on fluorescence of diluted stock), indicating a 25-fold PSA enrichment within just 1.2 s of nDEP, with further steady enrichment over time (Figure 3e-3f). Fluorescence images in the molecular dam region with immobilized anti-PSA, prior to and following PSA enrichment after a PBS wash step (Figure 3g and 3h, respectively), confirm a significant degree of

enhancement in PSA binding. The measurement of PSA enrichment by fluorescence analysis is limited by non-specific binding (Figure 3h) and the limited path length of light within the nanoslit, which limits sensitivity to the ~µg/mL range.

Influence of PSA enrichment on binding kinetics to anti-PSA

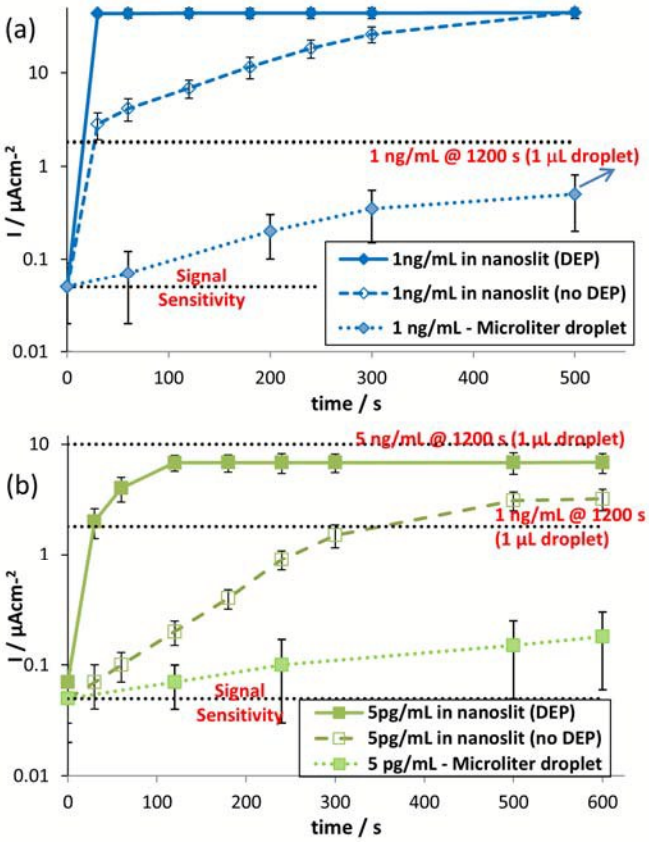

Fig. 4: Comparing PSA binding kinetics with immobilized anti-PSA within: (i) microliter droplet (dotted line & dotted symbols); (ii) nanoslit device in absence of nDEP enrichment (dashed lines & open symbols); (iii) nanoslit device with nDEP enrichment (solid lines & solid symbols) at PSA levels of: (a) 1 ng/mL: diamond symbols; and (b) 5 pg/mL: square symbols. Standard deviations are from three independent voltammetric measurements and the signal background determines the signal sensitivity at: 0.05 µA/cm^2. The signal levels achieved with 1 ng/mL and 5 ng/mL PSA at steady state (1200 s) using the microliter droplet incubation method (i) are shown as horizontal dotted lines for comparison with other methods (ii and iii).

For studying the binding kinetics of PSA to anti-PSA at concentration levels just below their k_d value, we choose electrochemical methods since their signal sensitivity is not limited due to analysis within the nanoslit. Furthermore, the voltammetric signal is not influenced by non-specific PSA adsorption at high surface area to volume regions of the nanoslit, since these are not proximal to the working electrode. Specifically, Figure 4 summarizes voltammetry data for detection inside: (i) ~1 µL scale droplet (dotted lines); (ii) the nanoslit device without nDEP enrichment (dashed lines); and (iii) the nanoslit device with nDEP enrichment (solid lines). The voltammetry platform shows a wide signal range, from a sensitivity of ~0.05 µA/cm^2 to a signal saturation level of: ~45 µA/cm^2. We choose the PSA concentration levels of 1 ng/mL (Figure 4a: blue curves) and 5 pg/mL (Figure 4b: green lines), since these fall just at and below the k_d value for PSA binding to anti-PSA [8], thereby making it possible to discern clearer differences in binding rate by addressing mass transport limitations. For case (i), the slow binding kinetics of PSA to anti-PSA in this concentration range is apparent from the rather slow rise in signal versus time. With 1 ng/mL of PSA (Figure 4a: blue dotted curve), the signal rises above the background level only after ~200 s of binding time, reaching a steady-state level of 1.8 µA/cm^2 after 1200 s (blue dotted horizontal line). With PSA at 5 pg/mL in the microliter droplet (Figure 4b: green dotted curve), the detection is ambiguous until ~600 s of binding time, due to the large standard deviations at earlier times and due to the absence of a clear saturation in signal within the maximum measurement time of 1200 s. The respective steady-state signal level after a binding time of 1200 s with 1 ng/mL and 5 ng/mL PSA, are shown for reference (Figure 4b: black dotted horizontal lines at 1.8 and 10 µA/cm^2, respectively). For case (ii), the rapid enhancement of binding kinetics of PSA to anti-PSA immobilized inside the nanoslit is apparent from the sharp rise in signal within the first time point (~30s of binding time) at PSA levels of 1 ng/mL (Figure 4a: dashed blue curve) and 5 pg/mL (Figure 4b: dashed green curve), with signal saturation at ~500 s. Also, apparent is the reduction in standard deviation of the signals, especially as the signals approach a steady-state level of target binding to immobilized capture probes. For case (iii) under nDEP enrichment of PSA inside the nanoslit, the signal exhibits an even sharper rise, and reaches its steady-state level within 120 s with 5 pg/mL PSA (Figure 4b) and at well less than 30 s with 1 ng/mL PSA. It is also apparent that the standard deviations for the respective signals are minimal, especially as the signals approach their steady-state value.

Overall, enhancement of the binding kinetics causes signal saturation at a higher level and at significantly earlier times, with a higher level of enhancement for binding in the nanoslit versus the microliter droplet and further enhancement upon nDEP enrichment of PSA in the nanoslit. At detection limit levels, the onset of steady-state binding conditions is determined by the equilibrium between analyte association and dissociation [46], rather than by saturation of the immobilized capture probes. Hence, the steady-state signal at detection limit analyte levels can be increased by shifting the equilibrium in favor of analyte association [11], either by creating a concentrated analyte plug through nDEP enrichment of PSA and/or by enabling more effective analyte capture at the binding surface, as achieved within the nanoslit geometry under electrokinetic flow. In this manner, by enabling nDEP enrichment in the nanoslit we can avail both these methods to further enhance the net signal saturation level. However, the net concentration level achieved under nDEP enrichment in the nanoslit drops with the starting PSA level, as apparent from the drop in steady-state signal level, even as the time to reach steady-state seems somewhat unchanged. Hence, while the

steady-state signal level with 1 ng/mL PSA is enhanced under nDEP enrichment in the nanoslit from ~1.8 μA/cm^2 (within μL droplet) to ≥40 μA/cm^2, which corresponds to signal from the near-complete binding of capture probes, the signal enhancement with 5 pg/mL PSA is more modest, with a steady-state signal level of ~7 μA/cm^2. Furthermore, the steady-state signal level using the nanoslit geometry with no nDEP enrichment is significantly lower (~3 μA/cm^2), suggesting a sharper influence of enhancement of concentration versus enhancement of analyte capture on shifting the equilibrium in favor of analyte association. The inability of nDEP enrichment to cause steady-state signals at the capture probe signal saturation level, even upon prolonged nDEP enrichment can be attributed to limitations from back-diffusion, electrothermal flow under Joule heating, and possibly from conformation incompatibility of some fraction of the enriched PSA molecules to immobilized anti-PSA. Hence, improvement of the detection sensitivity under nDEP enrichment is determined by whether this enhanced steady-state level falls above the signal sensitivity level. The degree of nDEP enrichment based on the steady-state signal is quantified in Figure 4b. A starting level of 5 pg/mL of PSA (green solid line or case (iii)) saturates within 120 s at a signal level similar to that achieved with free diffusion (case (i)) using 5 ng/mL PSA (black dotted line). This suggests that a dilute plug with 5 pg/mL PSA exhibits signal characteristics somewhat similar to a concentrated plug with ~1000x PSA enrichment in the vicinity of anti-PSA capture probes, due to nDEP trapping in the nanoslit device over 120 s.

Enhancing sensitivity for PSA detection

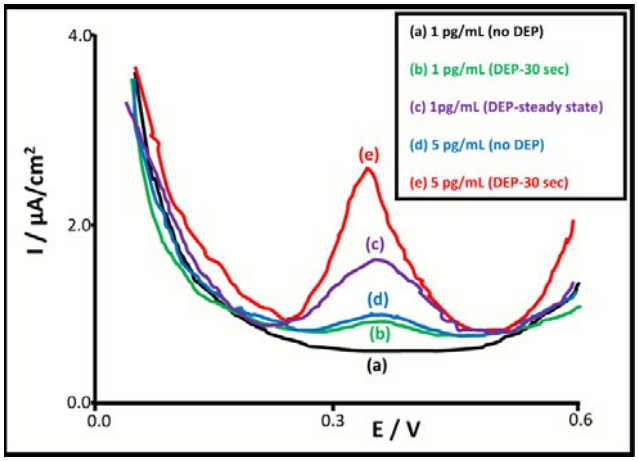

Fig. 5: Square wave voltammetry scans for PSA binding with anti-PSA immobilized in nanoslit device at PSA levels of 5 pg/mL (without and with nDEP enrichment over 30 s binding time in: d & e) and 1 pg/mL (without nDEP enrichment (a) and with nDEP enrichment for 30 s (b) and for 120 s (c)).

While enhancement of PSA binding kinetics under nDEP enrichment leads to earlier signal saturation, the net steady-state signal falls with lower starting PSA levels. Hence, we explore improvements to the limit of detection (LOD) based on whether the enhanced steady-state signal at lower PSA levels falls above signal sensitivity. From signal levels in Figure 4b, it is apparent that PSA detection at the 5 pg/mL level in the μL droplet is ambiguous, whereas it is clear within the nanoslit device and is further sped-up upon nDEP enrichment. This difference is also apparent in the voltammetric scans after 30 s of binding time with 5 pg/mL of PSA within the nanoslit device, in absence (Figure 5d) and with nDEP enrichment (Figure 5e). The signal levels (after 30 s binding time) are higher with nDEP enrichment and the standard deviations are lower (see Figure 4b: solid square symbol at 2 μA/cm^2 versus open square symbol at 0.08 μA/cm^2 that barely rises above the signal sensitivity). On the other hand, PSA levels of 1 pg/mL cannot be detected on the nanoslit device in the absence of nDEP enrichment (Figure 5a). After 30 s of nDEP enrichment in the nanoslit device, the signal barely rises beyond the sensitivity level (Figure 5b), while after 2 minutes of nDEP enrichment, a steady-state signal well above the background is apparent (Figure 5c). Hence, the earlier signal saturation caused by nDEP enrichment of PSA in the nanoslit, improves sensitivity to enable a 1 pg/mL detection limit in PBS media.

Comparison to standard immunoassay in serum samples

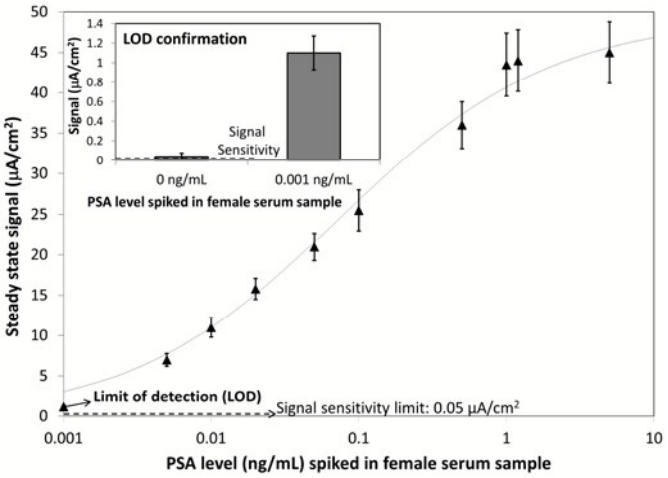

Fig. 6: Dilution plot (1 pg/mL – 5 ng/mL) based on steady-state signals (≥120 s of binding time under nDEP enrichment) from female serum samples spiked with PSA (net media conductivity is 1.5-1.6 S/m). The data are fit to a standard sigmoidal curve computed by a five-parameter logistic regression model. Inset shows confirmation of LOD (blank±3σ). Raw voltammetric scans at 50, 10 and 5 pg/mL are in Supporting Information.

The steady-state voltammetric signal level after nDEP enrichment in the nanoslit was correlated to the starting PSA concentration by using the dilution plot in Figure 6, which was determined by spiking PSA into the female serum sample for net levels between 1 pg/mL to 5 ng/mL, within media of ~1.5 S/m conductivity. Example voltammetric scans at 50, 10 and 5 pg/mL are shown in Supporting Information. At 50 pg/mL PSA, steady-state signal levels after nDEP enrichment are higher (~22 μA/cm^2) versus without nDEP enrichment (~17 μA/cm^2) in the nanoslit, similar to the trend observed with 5 pg/mL PSA in PBS media (~7 μA/cm^2 vs. ~3 μA/cm^2 in Fig. 5b). Voltammetric scans at 10 pg/mL and 5 pg/mL (Supporting Information) show clear rise above the background (female

serum sample). It is noteworthy that the signal levels for 1 ng/mL PSA in serum in Figure 6, at ~43 μA/cm^2, are close to those obtained using 1 ng/mL in PBS media (Figure 4a). Also, the inflection towards the LOD at 1 pg/mL PSA levels in serum (Figure 6) is equivalent to the signal level from 1 pg/mL in PBS media (Figure 5c). The inset to Figure 6 shows confirmation of the LOD at 1 pg/mL, by comparing the "blank" measurement signal without any spiked PSA plus 3 standard deviations to that from a sample with 1 pg/mL spiked PSA, which shows significantly higher signals. It is noteworthy that since spiked PSA levels > 5 ng/mL reach their steady state signal almost immediately (within a few seconds), they are not well-quantified by the reported nDEP enrichment method, due to insignificant signal modulation with increasing PSA levels. The reported assay with nDEP enrichment within the nanoslit geometry was benchmarked against a clinically validated 2-step immunoassay using three de-identified PSA samples at: 0.22 ng/mL (Sample 3), 0.55 ng/mL (Sample 1) and 1.82 ng/mL (Sample 4). For this purpose, the serum samples were diluted ~10-fold within PBS to bring the final media conductivity to ~1.5 S/m and then analyzed by square wave voltammetry in the nanoslit, as per voltammetric scans in Supporting Information, Figure SI-3(i). The dilution plot of Figure 6 was then used to correlate the determined signal with a respective PSA level, after accounting for the dilution of the original sample. The comparison in Table 1 at original PSA level after accounting for dilution shows a high level of correspondence between the two assays at the lower PSA levels of 0.22 ng/mL (Sample 3) and 0.55 ng/mL (Sample 1), with more significant differences at the higher PSA levels (1.82 ng/mL by Abbott Architect versus 1.95 ng/mL by the reported assay). The correspondence would likely be lowered, with increasing number of analytical runs on the Abbott Architect system. It is noteworthy that 5-fold dilution levels can also be used, but the lower net media conductivity (~1.3 S/m) caused the voltammetric scans to exhibit a rise in the background levels with voltage, as apparent for sample 3 in Supporting Information Figure SI-2(ii).

Table 1: Comparison of PSA levels determined from the reported assay versus a standard two-step immunoassay. Errors are from three measurements on the reported assays.

Sample #	2-step immunoassay	Reported assay
3	0.22 ng/mL	0.20±0.019 ng/mL
1	0.55 ng/mL	0.50±0.037 ng/mL
4	1.82 ng/mL	1.95±0.073 ng/mL

4 Conclusions

We address the mass transport limitations of the analyte within heterogeneous immunoassays to enable rapid signal saturation for improving detection accuracy and enhance the steady-state signal level to improve the detection limit. This is accomplished by nanoslit confinement strategies to eliminate diffusion boundary layers, as well as by creating a highly concentrated plug of the biomarker in the nanoslit, through enrichment under the molecular dam scheme with negative dielectrophoresis (nDEP). Our specific conclusions are: (1) Prostate Specific Antigen (PSA) biomarkers can be significantly enriched within just a few seconds (~25-fold preconcentration in just over a second) in regions away from sharp lateral constrictions in a nanoslit device, using a 6 MHz AC field of 200 V_{pp}/cm alongside a 1.5 V/cm DC field. (2) The nDEP enriched PSA biomarkers can effectively bind to anti-PSA capture probes immobilized on the nanoslit device. (3) Comparing the binding kinetics of PSA (5 pg/mL – 1 ng/mL range) to anti-PSA in a microdroplet versus on a nanoslit device, with and without nDEP enrichment, we show the steep enhancement in signal versus time on the nanoslit platform, with steady-state signal levels achieved within just 2 minutes upon nDEP enrichment. We suggest that the localized concentration enhancement caused under nDEP enrichment of PSA shifts the equilibrium in favor of analyte association with anti-PSA capture probes to result in a sharp signal rise over time, whereas the enhanced radial diffusion in the nanoslit geometry causes a more modest signal rise over time by enabling more effective analyte capture at the binding surface. However, the ability of nDEP enrichment over a prolonged duration in the nanoslit to cause binding at saturation levels of capture probes is limited by back-diffusion, electrothermal flow under Joule heating, and possibly from conformation incompatibility of some fraction of the enriched PSA molecules to immobilized anti-PSA. Hence, improvement of the detection sensitivity is dictated by whether the enhanced steady-state signal falls above the signal sensitivity level, which we show is the case down to 1 pg/mL PSA in PBS media using nDEP enrichment in the nanoslit coupled to the electrochemical assay. Using a dilution plot of PSA in female serum, we show correspondence of the reported assay to a standard two-step immunoassay for three de-identified samples. Based on reduced standard deviation of signals at early time points and the relative insensitivity of signals to incubation time at later time points, we envision more accurate immunoassays in nanoslits.

5 Acknowledgements

This work was supported by AOARD grant #114083 and FA2386-12-1-4002, NSF EAPSI program, Academia Sinica Nano Program and Integrated Thematic Project (AS-103-TP-A01), and the Ministry of Science and Technology, Taiwan (102-2112-M-001-005-MY3 and 103-2923-M-001-007-MY3). We thank the technical support from AS Nano Core Facilities.

6 Notes

a – Department of Electrical & Computer Engineering, University of Virginia, Charlottesville, Virginia-22904, USA
b – Institute of Physics, Academia Sinica, Taipei-11529, Taiwan.
c – Department of Pathology, University of Virginia, Charlottesville, Virginia-22904, USA
* Corresponding authors: nswami@virginia.edu, cfchou@phys.sinica.edu.tw

7 References

[1] B. Chikkaveeraiah, A. Bhirde, N. Morgan, H. Eden, and X. Chen, *ACS Nano*, 2012, 6, 6546-6561.
[2] M. -I. Mohammed and M. P. Y. Desmulliez, *Lab. Chip*, 2011, 11, 569-595.
[3] J. F. Rusling, *Chem. Rec.* 2012, 12, 164-176.
[4] A.C. Fan, D. Deb-Basu, M.W. Orban, J. R. Gotlib, Y. Natkunam, R. O'Neill, R. A. Padua, L. W. Xu, D. Taketa, A. E. Shirer, S. Beer, A. X. Yee, D. W. Voehringer, and D. W. Felsher, *Nat. Med.*, 2009, 15, 566-571.
[5] G. Hu, Y. Gao, and D. Li, *Biosens Bioelectron.*, 2007, 22, 1403-1409.
[6] P.R. Nair and M. A. Alam, *Appl. Phys. Lett.*, 2006, 88, 233120:1-3.
[7] R. Karlsson, P. S. Katsamba, H. Nordin, E. Pol, and D.G. Myszka, *Anal. Biochem.* 2006, 349, 136-147.
[8] Y. Uludag and I.E. Tothill, *Anal. Chem.*, 2012, 84, 5898−5904.
[9] H. C. Alphonsus, U. Uddayasankar, and A.R. Wheeler, *Anal. Bioanal. Chem.* 2010, 397, 991-1007.
[10] A. Bange, H. B. Halsall, and W. R. Heineman, *Biosens. Bioelectron.* 2005, 20, 2488-2503.
[11] M. Zimmermann, M. Wolf, E. Delamarche, and P. Hunziker, *Biomed. Microdevices*, 2005, 7, 99-110.
[12] P. E. Sheehan, L. J. Whitman, *Nano Lett.*, 2005, 5, 803-807.
[13] H. Parsa, C. D. Chin, P. Mongkolwisetwara, B. W. Lee, J. J. Wang, and S. K. Sia, *Lab Chip*, 2008, 8, 2062-2070.
[14] S. J. Kim, Y. -A. Song, and J. Han, *Chem. Soc. Rev.* 2010, 39, 912-922.
[15] Y. C. Wang and J. Han, *Lab Chip*, 2008, 8, 392-394.
[16] L. F. Cheow, S. H. Ko, S. J. Kim, K. H. Kan, and J. Han, *Anal. Chem.*, 2010, 82, 3383–3388
[17] N. F. Y. Durand and P. Renaud, *Lab Chip*, 2009, 9, 319-324.
[18] R. B. Schoch, L. F. Cheow, and J. Han, *Nano Lett.*, 2007, 7, 3895-3900.
[19] D. Holmes, K. S. Joseph, P. L. Roach, and H. Morgan, *Lab Chip*, 2007, 7, 1048-1056.
[20] J. Ramón-Azcón, R. Kunikata, F. -J. Sanchez, Marco, M.-P., Shiku, H., Yasukawa, T., Matsue, T., 2009 Biosens. Bioelectron. 24, 1592-1597.
[21] K. T. Liao, and C. F. Chou, *J. Am. Chem. Soc.* 2012, 134, 8742-8745.
[22] K. T. Liao, M. Tsegaye, V. Chaurey, C. F. Chou, and N. S. Swami, *Electrophoresis*, 2012, 33, 1958-1966.
[23] B. J. Sanghavi, W. Varhue, J. L. Chavez, C. F. Chou, N. S. Swami, *Anal. Chem.*, 2014, 86, 4120-4125.
[24] B. J. Sanghavi, O. S. Wolfbeis, T. Hirsch, N. S. Swami, *Microchim. Acta*, 2015, 182, 1-41.
[25] V. Chaurey, C. F. Polanco, C. F. Chou, N. S. Swami, *Biomicrofluidics*, 2012, 6, 012806.
[26] N. S. Swami, C. F. Chou, V. Ramamurthy, V. Chaurey, *Lab Chip*, 2009, 9, 3212-3220.
[27] N. S. Swami, C. F. Chou, and R. Terberueggen, *Langmuir*, 2005, 21, 1937-1941.
[28] V. Chaurey, A. Rohani, Y.-H. Su, K. T. Liao, C. F. Chou, and N. S. Swami, *Electrophoresis*, 2013, 34, 1097-1104.
[29] T. Leichléa, Y. -L. Lin, P.-O. Chiang, S. -M. Hu, K. -T. Liao, and C. -F. Chou, *Sens. Actuators B*, 2012, 161, 805-810.
[30] A. Rohani, W. Varhue, Y.-H. Su, and N. S. Swami, *Biomicrofluidics*, 2014, 8, 052009.
[31] V. Farmehini, A. Rohani, Y.-H. Su and N. S. Swami, *Lab Chip*, 2014, 14, 4183 - 4187.
[32] B. V. Chikkaveeraiah, V. Mani, V. Patel, J. S. Gutkind, and J. F. Rusling, *Biosens. Bioelectron.*, 2011, 26, 4477-4483.
[33] B. Jeong, R. Akter, O. H. Han, C. K. Rhee, and M. A. Rahman, *Anal. Chem.*, 2013, 85, 1784-1791.
[34] J. Gu, R. Gupta, C.-F. Chou, Q. Wei, and F. Zenhausern, *Lab Chip*, 2007, 7, 1198-1201.
[35] T. Leichléa and C. F. Chou, *Biomicrofluidics*, 2015, 9, 034103.
[36] N. E. Hebert, B. Snyder, R. L. McCreery, W. G. Kuhr, S. A. Brazill, *Anal. Chem.*, 2003, 75, 4265-4271.
[37] S. -J. Li, D. -H. Deng, Q. Shi, S. -R. Liu, *Microchim. Acta*, 2012, 177, 325-331.
[38] B. J. Sanghavi, S. Sitaula, M. H. Griep, S. P. Karna, M. F. Ali, and N. S. Swami, *Anal. Chem.*, 2013, 85, 8158-8165.
[39] B. J. Polk, A. Stelzenmuller, G. Mijares, W. MacCrehan, M. Gaitan, *Sens. Actuators B*, 2006, 114, 239-247.
[40] M. P. Chatrathi, J. Wang, G. E. Collins, *Biosens. Bioelectron.*, 2007, 22, 2932-2938.
[41] R. Liu, C. Wang, Q. Jiang, W. Zhang,Z. Yue and G. Liu, *Anal. Chim. Acta*, 2013, 801, 91-96.
[42] A. Rohani, W. Varhue, Y.-H. Su, and N. S. Swami; *Electrophoresis* (2014), 35, 1795-1802.
[43] B. Sweryda-Krawiec, H. Devaraj, G. Jacob, and J. J. Hickman. *Langmuir*, 2004, 20, 2054−2056.
[44] N. Swami and D.B. Dresinger. *Solvent Extr. Ion Exch.*, 1995, 13, 1037-1062.
[45] F. Persson, J. Fritzsche, K. U. Mir, M. Modesti, F. Westerlund, and J. O. Tegenfelt, *Nano Lett.*, 2012, 12, 2260−2265.
[46] D. Leboeuf and N. Henry. *Langmuir*, 2006, 22, 127-133.